11(2014) 223 – 244



Latin American Journal of Solids and Structures
www.lajss.org

A new metamodel for reinforced panels under compressive loads and its application to the fuselage conception

Abstract

This work presents a new metamodel for reinforced panels under compressive loads, typically used in light-weight aircraft structures. The metamodel represents a replicable cell structure of integrally machined panels. The presented formulation for conception is based on the synthesis of four stability criteria: section crippling, web buckling, flange buckling and column collapse. The aluminum alloy, a typical choice in modern aircraft industry, is selected and the structure is expected to work in the linear elastic domain. In order to evaluate the accuracy and to validate the analytical tool, the procedure is applied in the pre-sizing of the fuselage basic structural components of a 9-passenger executive aircraft. The pull-up maneuver, one of the critical load conditions in most of aircrafts, causes the maximum compressive stresses in lower fuselage panels. Finite element models are presented to the resulting fuselage configuration. The optimal configuration achieved through the application of the analytical tool yields to an innovative structure from those usually adopted in the aeronautical industry. This structural configuration is presented and discussed. The developed metamodel proved to be effective, presenting satisfactory results with adequate accuracy for the initial stages of light-weight aircraft structure.

Keywords

structural optimization, structural stability, reinforced panels

Alessandro Teixeira Neto*
Flávio Luiz de Silva Bussamra**
Henrique Araújo de Castro e Silva

Instituto Tecnológico de Aeronáutica, CTA - ITA - , São José dos Campos - SP 12228-900, Tel.: 55-12-39475977; Brazil.

Received in 30 Jan 2013
In revised form 21 May 2013

*Author email: alessandro.t.neto@uol.com.br
**Author email: flaviobu@ita.br

1 INTRODUCTION

Compressive loads acting on thin-walled structures, typically used in modern airframes, lead to failure by instability at stresses far below the material yielding compressive stress. In order to achieve the maximum structural efficiency, the designer and the structural engineer must arrange the structural elements wisely.

Stiffened panels stability is a fundamental issue to structural designers. Wang (1997) presented an approximated method for lateral buckling of thin-walled members, taking into account the shear lag phenomenon. The buckling in airplane wings and fuselages with FSW – friction stir welding – is analyzed by Yoon et al. (2009), for the elastic-plastic material behavior, where numerical simulations with Abaqus (2006) finite element code is presented. The buckling analysis of fuselage stiffened panels loaded in compression is also simulated in Abaqus by Lynch et al. (2004). Non-linearity in the post-buckling thin-walled panels is discussed by Alinia et al. (2009) and Stamatelos et al. (2011). Analytical results in linear buckling of multi-stiffened panels under compression are presented by Bedair (1997), and Kolakowski and Teter (2000).

The airframe conception poses a complex duty to the product development engineering. It is expected to an efficient arrangement of the structural elements the capability to endure the loads that the aircraft are subjected to and also to cover its whole external surface at the least mass cost. It is a paradox, i.e. opposite expectations which can be overcame only by searching for the best compromise solution between light weight and high mechanical strength of the airframe. Analyses through the available computational packages are very helpful to the engineers. For many problems, however, a single simulation can take many minutes, hours, or even days to complete. As a result, routine tasks such as design optimization, design space exploration, sensitivity analysis and what-if analysis become impossible since they require thousands or even millions of simulation evaluations.

One way of alleviating this burden is by constructing approximation models, such as surrogate models and metamodels. They mimic the behavior of the simulation model as close as possible while being computationally cheaper to evaluate. Surrogate models (Forrester et al., 2008; Toropov, 2013) are built using a data-driven, bottom-up approach. The exact, inner working of the simulation code is not assumed to be known (or even understood), solely the input-output behavior is important. So, a model is constructed based on modeling the response of the simulator to a limited number of intelligently chosen data points.

Metamodeling in engineering, mathematics, among other disciplines, is the analysis, construction and development of the frames, rules, constraints, models and theories applicable and useful for modeling a predefined class of problems. In other words, metamodeling is the construction of a collection of concepts (things, terms etc.) within a certain domain. A model is an abstraction of the phenomena in the real world; and a metamodel is yet another abstraction, highlighting properties of the model itself. The simplest metamodel in structural analysis is the one representing a truss bar. Truss structures are ubiquitous in the industrialized world, appearing as bridges, towers, roof supports and building exoskeletons, yet are complex enough that modeling them by hand is time consuming and tedious. Trusses are represented as a set of rigid bars connected by pin joints, which may change location during optimization. By knowing the metamodel behavior – compressive strength and stiffness – of a single truss as a function of the slenderness ratio of the bars, it is possible to simultaneously optimize the geometry and the mass of structures (Smith et al., 2013). Lee and Kang (2007) presented the metamodeling of back-propagation neutral network, illustrated by truss optimization examples. Caseiro et al. (2011) presented non-linear metamodeling buckling analysis of integrally stiffened panels.

The present methodology for the pre-sizing of reinforced panels under compressive loads is based on the synthesis of four stability criteria in the simple metamodel depicted in Fig. 1. It represents a typical part of fuselage or wing box. For riveted reinforcements, it is clearly a rough approximation model, but it is quite the exact representation of modern integrally machined panels. The basic geometric parameters of the metamodel for the reinforced panel are: the panel length L, the web width b_s and thickness t_s, and the flange height b_w and thickness t_w. The panel is made of aluminum and is expected to work in the linear elastic domain. Four stability criteria are taken into account: section crippling, web buckling, flange buckling and column collapse.

The objective of this article is to present an efficient metamodel for reinforced panels under compressive loads, typically used in light-weight aircraft structures. Non-buckling panels are the design criteria herein adopted, so this method is not comparable with post-buckling methods of analysis, like effective width, global/local finite element methods or material equivalent plasticity for buckling of beams with flat webs.

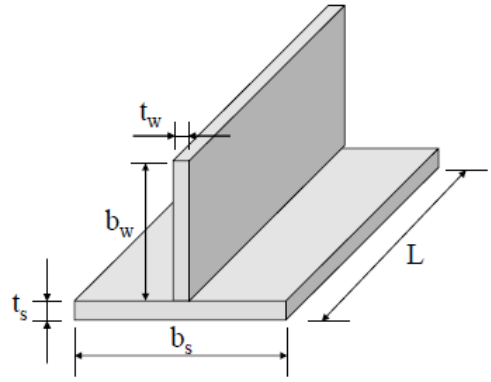


Figure 1 Metamodel of the reinforced panel under compression.

To illustrate the use of the metamodel, two numerical applications are presented: a) the optimization of a reinforced flat panel under compressive load and b) the pre-sizing of a typical semimonocoque center fuselage of a 9-passenger aircraft, subjected to pull-up maneuver, which leads to the highest compressive loading in these lower fuselage panels. Both resulting structures are then modeled in MSC/Nastran (2004) finite element code in order to evaluate its behavior.

2 METAMODEL ANALYSIS

The following stability criteria are considered to the design of the metamodel presented in Fig. 1. The presented formulation is valid for aluminum alloys bars and panels.

2.1 Section Crippling

The crippling allowable stress F_{cc} of an arbitrary section under compressive load can be evaluated by Gerard Method (Lundquist and Stowell, 1941):

$$\frac{F_{cc}}{F_{cy}} = \beta\left[\left(\frac{gt^2}{A}\right)\sqrt{\frac{E}{F_{cy}}}\right]^m \tag{1}$$

where A is the cross-section area and t is the section thickness; m, g and β are dependent on the specific section shape. For a T-section with straight unloaded edges they result in g=3, $\beta = 0.67$ and m = 0.40. Since the panel geometry presents independent web thickness t_s and flange thickness t_w, the mean section thickness t is calculated as:

$$t = \frac{t_w b_w + t_s b_s}{b_w + b_s} \tag{2}$$

Additionally Gerard (1958) recommends the cut-off of crippling allowable stress at 0.8 F_{cy}.

2.2 Web and flange buckling

The web and the flange are considered as simple supported plates under axial loads in accordance with plate theory (Timoshenko and Gere, 1961). Although the most recent methods of post-buckling analysis include local stiffness of stringer and frame, this constraint condition is a choice to ease and to enhance the efficacy of the algorithm. The actual condition is known to be intermediary between simple supported and fixed for aeronautic skins and stringers. In conceptual or pre-sizing analysis, adopting the conservative condition; i.e., the simple supported condition, assures that the structure will be able to support the loads it has been designed for.

Figure 2 presents the geometry of a generic plate and its loads, where a and b are the element length and its width, respectively.

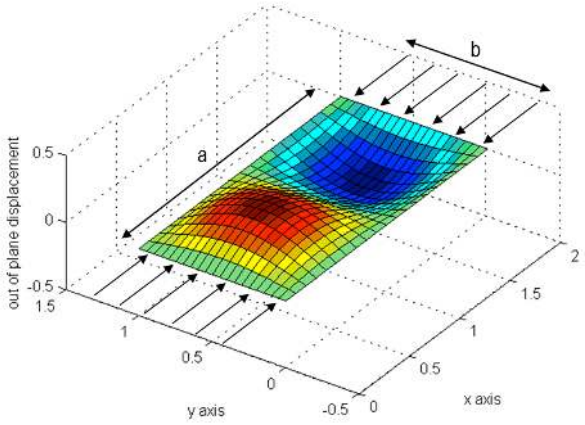


Figure 2 Out of plane buckling of a simple supported plate under axial loading.

The buckling failure stress F_{cb} of a plate of thickness t under axial loading is given by

$$F_{cb} = \frac{K_c \pi^2 E}{12\left(1-\nu^2\right)}\left(\frac{t}{b}\right)^2 \tag{3}$$

where K_c is the buckling coefficient, which is dependent on the plate boundary conditions. For a simple supported plate, or the panel web, it can be calculated by

$$K_c = \left(\frac{nb}{a} + \frac{a}{nb}\right)^2 \tag{4}$$

where n represents the sequence of integers from 1 up to infinity. So, Eq. (4) defines a series of $K_c(n)$ values for each ratio a/b of the panel. The effective buckling coefficient K_c is the lowest value of this series; $K_c = 4.0$ can be assumed for practical purposes if $a/b > 4$.

Lundquist and Stowell (1941) presents the buckling coefficient K_c for a simple supported flange:

$$K_c = \frac{6}{\pi^2}\left(1-\nu\right) + \left(\frac{b}{a}\right)^2 \tag{5}$$

The equalization of the buckling allowable stress of the web F_{cb_web} to the buckling allowable stress of the flange F_{cb_flange} yields

$$4\left(\frac{t_s}{b_s}\right)^2 = \frac{6}{\pi^2}\left(1-\nu\right)\left(\frac{t_w}{b_w}\right)^2 + \left(\frac{t_w}{L}\right)^2 \tag{6}$$

It must be observed that Eq. (6) leads to a dependency of the flange height b_w on the remaining variables of panel geometry (L, b_s, t_s, t_w) as a result of the concurrence of web and flange buckling design criteria, given by

$$b_w = \frac{t_w}{\pi}\sqrt{6\left(1-\nu\right)}\left[4\left(\frac{t_s}{b_s}\right)^2 - \left(\frac{t_w}{L}\right)^2\right]^{-1/2} \tag{7}$$

2.3 Column collapse

The panel is considered as a simple supported column under axial loads in accordance with Euler theory (Bruhn, 1973). The Euler formula for the column allowable stress F_{cr} is

$$F_{cr} = \frac{\pi^2 E}{\left(L'/\rho\right)^2} \tag{8}$$

where (L'/ϱ) is the slenderness ratio, calculated by

$$\left(\frac{L'}{\rho}\right)^2 = \frac{L^2 A}{I_x} \tag{9}$$

where the cross section area A of the panel is

$$A = t_w b_w + t_s b_s \tag{10}$$

and the inertia moment I_x is given by

$$I_x = \frac{t_s^3}{3}\left(b_s - t_w\right) + \frac{t_w}{3}\left(b_w + t_s\right)^3 - A\overline{y}^2 \tag{11}$$

with

$$\overline{y} = \frac{1}{A}\left[\frac{t_s^2}{2}\left(b_s - t_w\right) + \frac{t_w}{2}\left(b_w + t_s\right)^2\right] \tag{12}$$

2.4 The optimization procedure

The equivalent thickness t_{eq} given by

$$t_{eq} = \frac{A}{b_s} = \frac{b_s t_s + b_w t_w}{b_s} \tag{13}$$

is directly related to the resulting mass of the panel. The compressive allowable stress F_c can be defined as the minimum stress between those evaluated, regarding each one of the four criteria previously discussed that concur to the structural stability, i.e.

$$F_c(L, b_s, b_w, t_s, t_w) = \min\left(F_{cb_web}, F_{cb_flange}, F_{cc}, F_{cr}\right) \tag{14}$$

The Objective Function of maximizing $E_{ff} = F_c/t_{eq}$ is defined by

$$\begin{cases} \max\left\{E_{ff}(L,b_s,b_w,t_s,t_w)\right\} \\ E_{ff}(L,b_s,b_w,t_s,t_w) = \dfrac{F_c b_s}{A} \end{cases} \tag{15}$$

while the Design Space, usually found in typical wing and fuselage aluminum panels, is given by

$$\begin{cases} 0.1L \le b_s \le 0.4L \\ 0.005b_s \le t_s \le 0.2b_s \\ 0.5t_s \le t_w \le 2t_s \end{cases} \tag{16}$$

It must be observed that Eq. (15) enables the panel geometry to reach the best compromise solution between the maximum compressive allowable stress and the minimum mass, keeping coherence with the purposes of the dual nature of the problem.

2.5 Optimization results for AL7050-T7451

Equations (15) and (16) are applied to the metamodel made of aluminum alloy AL7050-T7451 Plate 2.75in, a typical choice in modern aircraft industry. Its mechanical properties are: elasticity modulus in compression $E = 73080$ MPa, Poisson coefficient $n = 0.33$ and yield compressive stress $F_{cy} = 421$ MPa. The optimization results are presented in Tab. 1. This set of results characterizes the panel geometry (t_w/t_s, t_s/b_s and t_w/t_s) and its respective compressive allowable stress F_c for a given value of the design parameter b_s/L.

Table 1 Metamodel for reinforced panels under compressive loads, AL7050-T7451.

b_s/L	b_w/b_s	t_s/b_s	t_w/t_s	F_c (MPa)	b_s/L	b_w/b_s	t_s/b_s	t_w/t_s	F_c (MPa)
0.10	0.5958	0.0328	1.8590	290.1	0.2500	0.2959	0.0321	0.9210	277.4
0.11	0.5452	0.0326	1.7010	286.2	0.2600	0.2885	0.0321	0.8980	277.7
0.12	0.5055	0.0324	1.5770	283.9	0.2700	0.2818	0.0321	0.8770	277.8
0.13	0.4729	0.0323	1.4750	282.1	0.2800	0.2751	0.0321	0.8560	277.8
0.14	0.4457	0.0323	1.3900	280.7	0.2900	0.2691	0.0321	0.8370	277.9
0.15	0.4223	0.0322	1.3170	279.6	0.3000	0.2637	0.0321	0.8200	278.3
0.16	**0.4025**	**0.0322**	**1.2550**	**278.9**	0.3100	0.2582	0.0321	0.8030	278.5
0.17	0.3849	0.0321	1.2000	278.4	0.3200	0.2532	0.0321	0.7870	278.7
0.18	**0.3696**	**0.0321**	**1.1520**	**278.0**	0.3300	0.2484	0.0321	0.7720	278.9
0.19	0.3559	0.0321	1.1090	277.7	0.3400	0.2439	0.0322	0.7580	279.0
0.20	0.3434	0.0321	1.0700	277.6	0.3500	0.2395	0.0322	0.7440	279.3
0.21	0.3322	0.0321	1.0350	277.5	0.3600	0.2353	0.0322	0.7310	279.4
0.22	0.3220	0.0321	1.0030	277.4	0.3700	0.2315	0.0322	0.7190	279.7
0.23	0.3125	0.0321	0.9730	277.3	0.3800	0.2277	0.0322	0.7070	279.9
0.24	0.3038	0.0321	0.9460	277.3	0.3900	0.2242	0.0322	0.6960	280.1

3 NUMERICAL APPLICATIONS

3.1 Five-flange reinforced panel under compressive load

An integrally machined panel with 5 flanges (4 panels) subjected to compressive loads is analyzed with the presented methodology. The optimized panel is built based on the metamodel parameters of the bolded line in Tab. 1, with $b_s/L = 0.18$. For L=500 mm and $b_s = 90$ mm, follow $t_s = 2.89$ mm, $b_w = 33.26$ mm, $t_w = 3.33$ mm and $F_c = 278.0$ MPa. Hence, the predicted critical load is $P_{c_theo} = 443.0$ kN.

A finite element model of integrally machined panel considering its optimal geometry is constructed in order to validate this theoretical result. The computational model is specially prepared for buckling analysis – Nastran solution 105 – presenting a total of 10,908 nodes and 10,700 shell elements CQUAD4 (isoparametric quadrilateral FE).

The numerical analysis resulted in a critical loading of $P_{c_num} = 458.9$ kN, i.e. a difference of only 3.6% is observed. Figure 3 presents the compressive stress distribution in the cover panel, and Fig. 4 presents the first failure mode of the structure. The simultaneous collapse of the panel regarding different stability criteria, as predicted by theory, can be verified.

It was observed to the optimized panel section that the allowable stresses according to the four stability criteria resulted in the same F_c value, which is around 2/3 of the material compressive yielding stress. Another relevant feature of this solution is that the panel geometry is scalable, i.e. the resulting compressive stress F_c for a given cross section (b_s/L, $b_w/\ b_s$, $t_s/\ b_s$, $t_w/\ t_s$) is fixed and isn't dependent on the panel length L.

Note, however, that the methodology is conservative when it assumes that the skin is sized as simply supported plate, the stringers as simply supported flanges and the panels as simply supported columns. Depending on the stiffness of the skin, stringers and frames, the buckling coefficient of reinforced panels can be greater than assumed in Tab. 1.

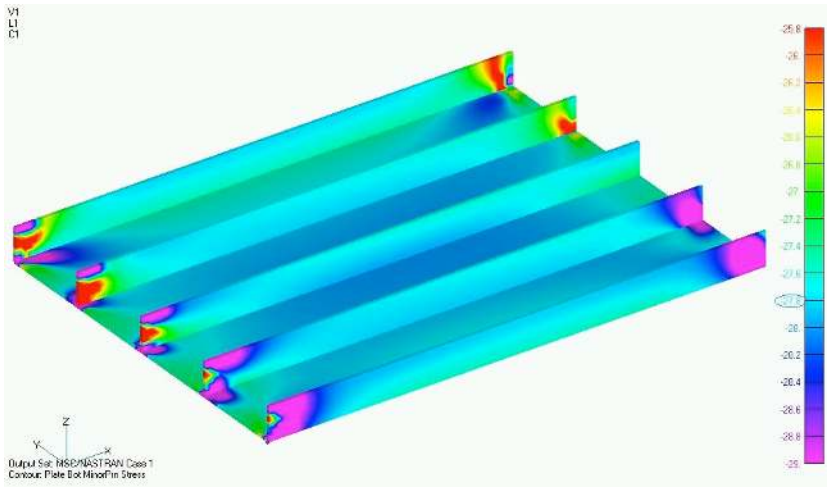


Figure 3 Compressive stress contour [×10MPa].

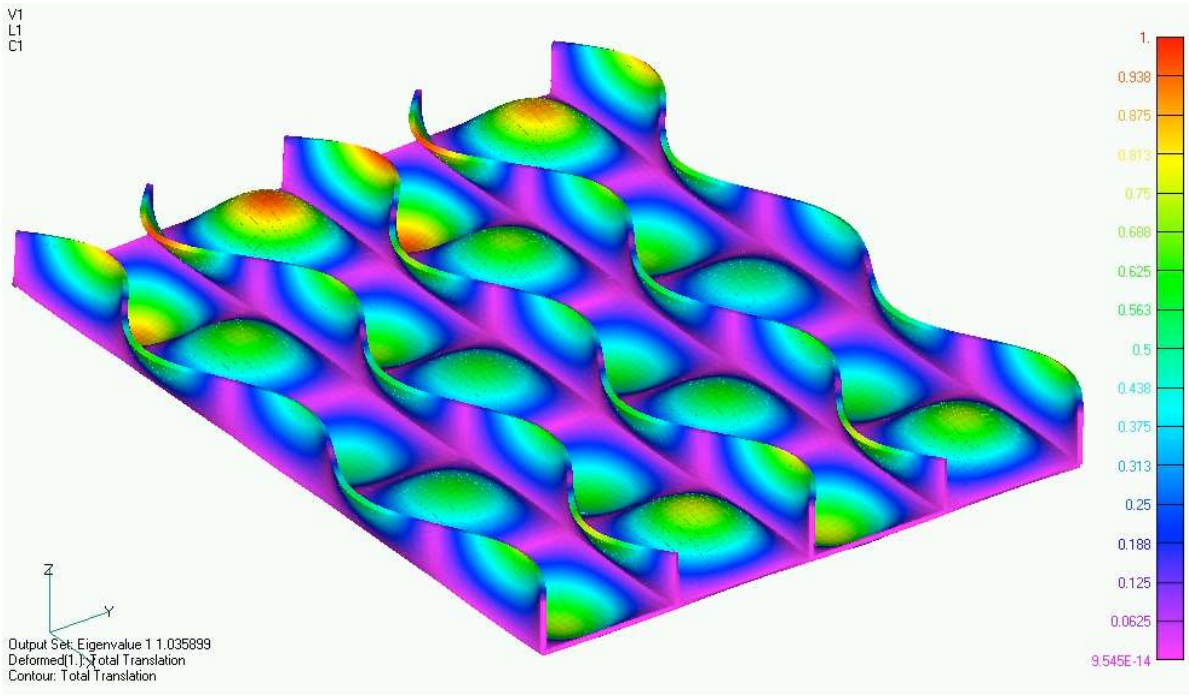


Figure 4 First buckling mode.

3.2 Scalability of the metamodel

J. Campbell et al. (2012) present an experimental and numerical analysis of a reinforced panel, subjected to compressive load. The panel consists of a rectangular plate of length 500 mm, width 492 mm and thickness 0.9 mm, stiffened by seven Z-shaped bars, as shown at Fig. 5. Stiffeners are revited on the plate. The plate and stiffeners are made of aluminum AL2014A-T6, which properties are: modulus of elasticity $E = 68$ GPa, Poisson's ratio $\nu = 0.33$, yield stress $F_y = 340$ MPa and mass density $\rho = 2{,}800$ kg/m^3. The collapse load is $P_c = 108.6$ kN. Its properties are listed at Tab. 2, column "Panel-a".

Although this panel is not optimized, it represents a typical fuselage airframe, so it is a good baseline to show the scalability of the metamodel. The panel dimensions are length $L = 500$ mm and width $b = 480$ mm. Four optimized panels are built based on the metamodel parameters of the bolded line in Tab. 1, with $b_s/L = 0.16$, web widths $b_s = 80$ mm, 40 mm, 20 mm and 16 mm (panels b_1, b_2, b_3 and b_4, respectively), all made of AL7050-T7451. The resulting panels properties are summarized at Tab. 2, and compared with airframe panel presented by Campbell et al (2012).

It can be noticed that all the panels b_i have the same Structural Efficiency of 197.1 kN/kg. In special, the Panel b_1, with 7 stringers (the same number as Panel-a) is of 1.84 times more structural efficient than Panel-a. By increasing the number of stringers, the mass decreases, and the collapse load P_c decreases proportionally. The choice of the number of stringers will also depend on the design loading and the design criteria other than buckling or material yielding (fatigue, damage tolerance, machining, vibration etc).

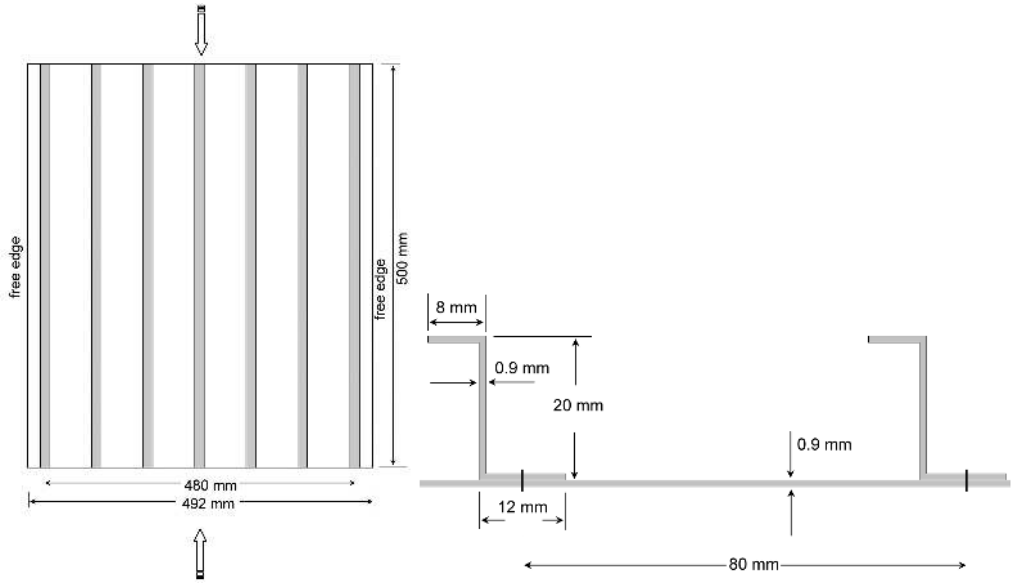


Figure 5 Top and side views of a typical airframe panel.

Table 2 Reinforced panels under compressive loads.

	Panel-a (Campbell, 2012)	Panel-b_1	Panel-b_2	Panel-b_3	Panel-b_4
L [mm] =	500	500	500	500	500
b [mm] =	480	480	480	480	480
b_s [mm] =	80.00	80.00	40.00	20.00	16.00
$N_{stringers}$ =	7	7	13	25	31
aluminum =	2014A-T6	7475-T7451	7475-T7451	7475-T7451	7475-T7451
t_s [mm] =	-	2.58	1.29	0.64	0.52
t_w [mm] =	-	3.23	1.62	0.81	0.65
b_w [mm] =	-	32.20	16.10	8.05	6.44
$A_{striger}$ [mm^2] =	34.38	104.10	26.02	6.51	4.16
A_{plate} [mm^2] =	72.00	206.08	51.52	12.88	8.24
V [mm^3] =	336330	982586	478280	235887	188189
mass [kg] =	0.9417	2.7807	1.3535	0.6676	0.5326
F_c [MPa] =	149.9	278.9	278.9	278.9	278.9
P_c [kN] =	100.83	548.09	266.78	131.58	104.97
Efficiency* =	107.07	197.10	197.10	197.10	197.10
% Mass** =	100.0%	295.3%	143.7%	70.9%	56.6%

* Structural Efficiency = P_c / Mass [kN/kg]

** % Mass = Mass / Panel-a mass

3.3 Executive aircraft fuselage

A midlight category executive aircraft, illustrated in Fig. 6, is utilized as the main application of this work. The aircraft presents a circular fuselage cross section, with configurations for 7 to 9 passengers. Figure 7 shows the fuselage segments: front fuselage, central fuselage and rear fuselage. The central fuselage segment, with 6.92 m long and a diameter of 2.10 m, is conceptually designed with the present metamodeling approach.



Figure 6 Executive aircraft under analysis.

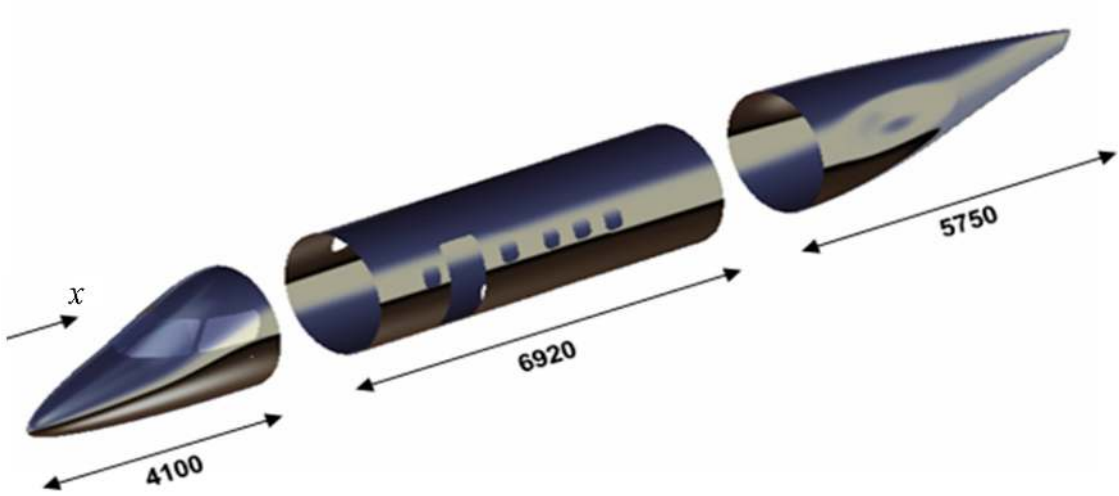


Figure 7 Fuselage segments

All the structural parts of the fuselage are made of aluminum alloy AL7050-T7451 Plate 2.75in, in accordance with Tab. 1. Only the pull-up maneuver load case is considered because it resulted in the highest values for bending moment and, hence, in the highest compressive stresses in the lower fuselage. This choice is acceptable for the fuselage conceptual design – its initial development stage. In a complete design cycle of the fuselage, all the load cases must be analyzed.

The ultimate load (1.5×limit load) is applied, since the failure mode in the context of this work, instability by different criteria, is assumed as being the failure of the whole fuselage. Eventual post-buckling behavior is disregarded. Figures 8 and 9 show the bending moment BMY and shear force SLZ, respectively, along the fuselage for the presented load case. The torsion moment is nil. The bolded curves refer to the part of the central fuselage under analysis. This region is limited by the connection of the central fuselage to the wing and by the connection to the rear fuselage, stations $x = 7.52$ m and $x = 11.02$ m, respectively.

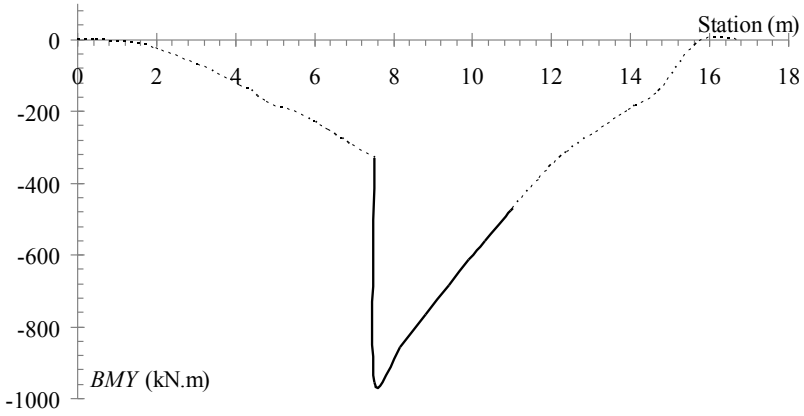


Figure 8 Bending moment diagram.

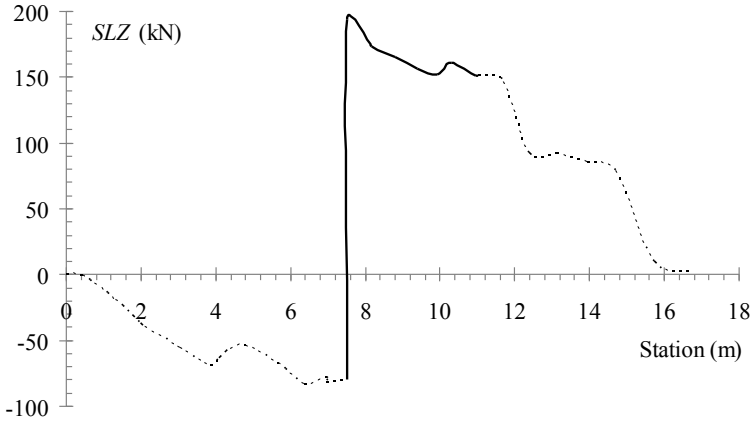


Figure 9 Shear force diagram.

3.3.1 Analytical Solution

By varying the number of stringers and the length of the panels, several geometric configurations of the fuselage are evaluated, until the optimal configuration from the standpoint of structural stability is reached. Figure 10 shows the distribution along the fuselage of the b_s/L parameter, according to Tab. 1 results, as input for setting the relations between the geometric variables that define the reinforced panel metamodel.

It can be seen that the parameter b_s/L grows from the connection of the central fuselage to the wing up to its connection to the rear fuselage, as the load decreases. Since it is assumed that the spacing between the stringers b_s in each bay is kept constant and the number of stringers does not change along the fuselage, the spacing between frames L reduces from the connection to the wing up to the rear fuselage. The spacing between stringers for the optimal design, which is constant around the cross section and along the fuselage, equals to $b_s = 13.74$ mm.

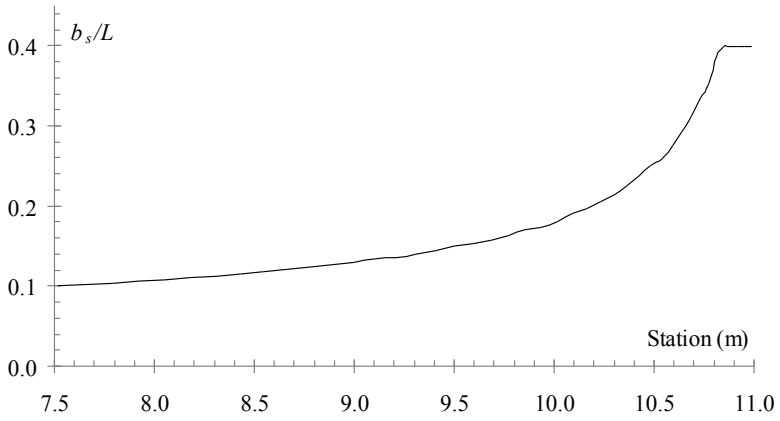


Figure 10 b_s/L distribution along the fuselage span.

Figure 11 shows the skin thickness t_s distribution along the fuselage span. The skin thickness is defined by the relation t_s/b_s, which varies itself with the input parameter b_s/L. It also can be noted that the skin thickness variation along the fuselage span, $0.44 < t_s < 0.45$ mm, is almost negligible.

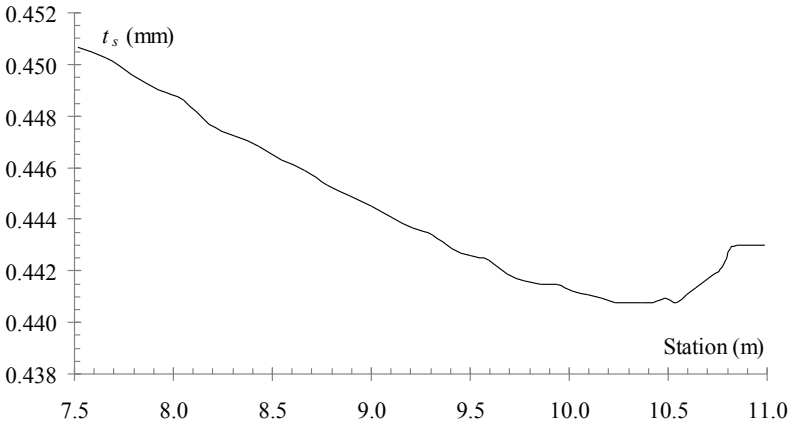


Figure 11 Skin thickness distribution along the fuselage span.

Figure 12 shows the distribution of skin, stringer and frame thicknesses, t_s, t_w, t_f, respectively, along the fuselage span, while the stringer height b_w distribution is shown in Fig. 13. It is noticed that the thickness and the height of the stringers decreases from the connection of the central fuselage to the wing up to the rear fuselage, following the reduction of the acting loads.

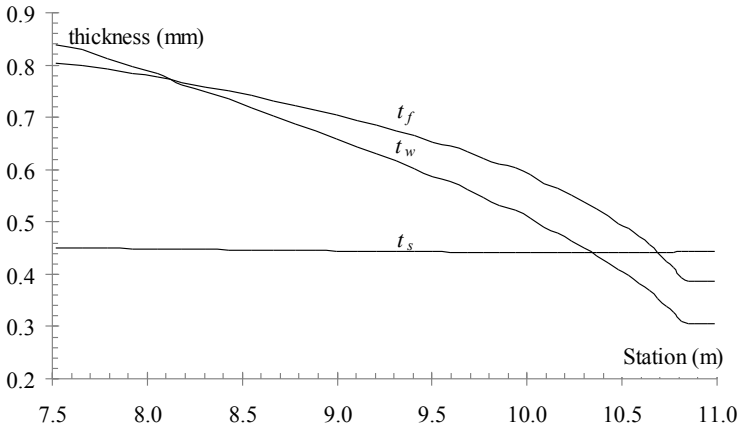


Figure 12 Stringer and frame thicknesses distribution along the fuselage span.

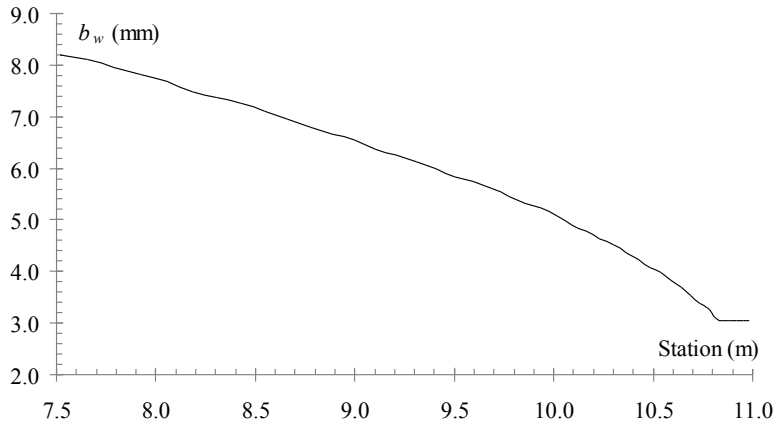


Figure 13 Stringer height distribution along the fuselage span.

It was decided that the frames should have the same height as the stringers of a certain bay, due to the innovative resulting geometry. So, Fig. 13 also presents the frame height distribution along the fuselage span. The resulting geometry alludes to a reticulated pattern of the structure. It is an option and trend that can lead to the manufacture of new aerospace structures. Although, the dimensions and spacing of the structural elements found herein make the fuselage manufacturing unfeasible considering current processes in the aeronautical industry nowadays.

Figure 14 shows the distribution of the ratio to the structural mass by panel length. As shown in Figs. 11 and 14 the skin thickness is almost constant along the fuselage span. Moreover, the frame mass is small if compared to the total mass of the fuselage and, thus, the reduction of the

total mass distribution of the structure is mostly due to the stringer mass variation. The b_s/L increase along the fuselage span, observed in Fig. 10, presents strong connection with the reduction of the stringer mass by the panel length, as well as with the almost invariable behavior of the frame mass by the panel length. Table 3 shows the final distribution of structural mass in the fuselage segment.

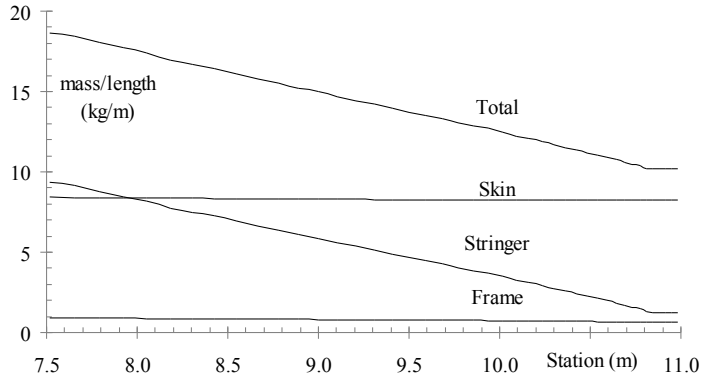


Figure 14 Distribution of the ratio to the structural mass by panel length.

Table 3 Structural mass distribution in the fuselage segment under analysis.

Component	Mass (kg)	% of the total mass
Stringers	18.6	37%
Frames	2.8	5%
Skin	29.1	58%
Total	50.4	100%

3.3.2 Finite element analysis

A global finite element model of the resulting fuselage designed in the previous item is built for linear static analysis in Nastran. Two load cases are applied: pressurization (for tensile verification) and pull-up maneuver loads (for pre-sizing analytical validation). Shell elements CQUAD4 were used to represent the fuselage skin and bar elements CBAR to represent the fuselage stringers and frames. Figure 15 shows a detail of the finite element mesh of the fuselage structure.

Ring connections with 200 mm length and 5 mm thickness are considered at the ends of the fuselage model. The model is constrained in its ring connection with the wing. Loads are applied on points in the center of the fuselage and distributed in the intersections of frames with stringers through rigid elements RBE3. An additional vertical force is applied on the $x = 14.118$ m station through rigid elements RBE3 attached to the ring connection with the rear fuselage in order to assure the bending moment and the shear force distributions according to Figs. 8 and 9.

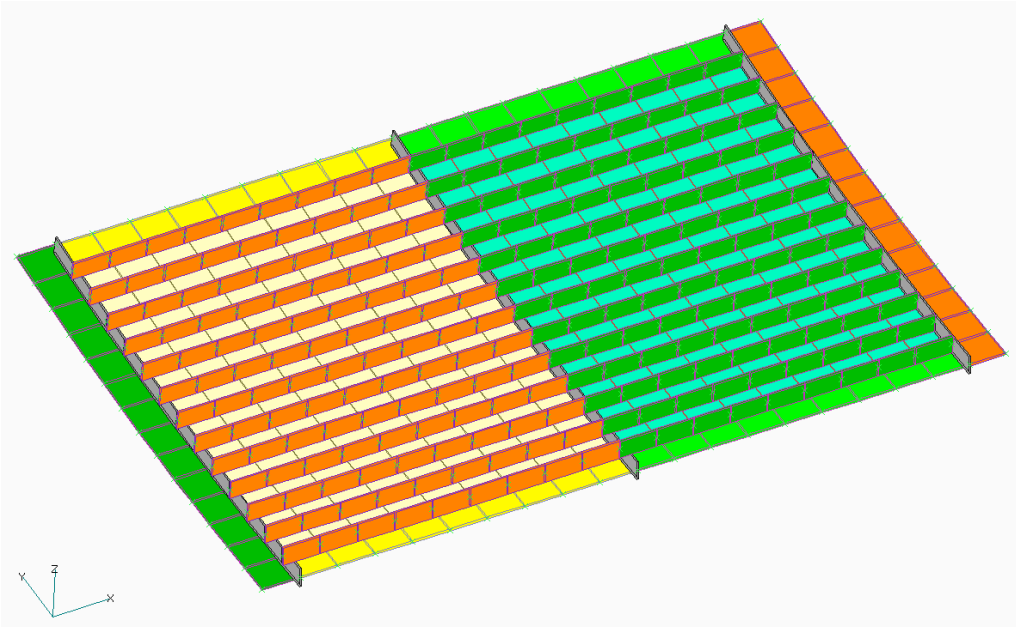


Figure 15 Finite element mesh of some panels of the fuselage.

The ultimate pressurization load, in accordance to the 25.365 item of the Federal Aviation Regulations - Part 25 (2011), is equal to $2\Delta P$ (0.14 MPa) and must be applied omitting other loads. Figure 16 presents the maximum combined stress distribution in the frames and Fig. 17 presents the Von Mises stress distribution in the reinforced panels.

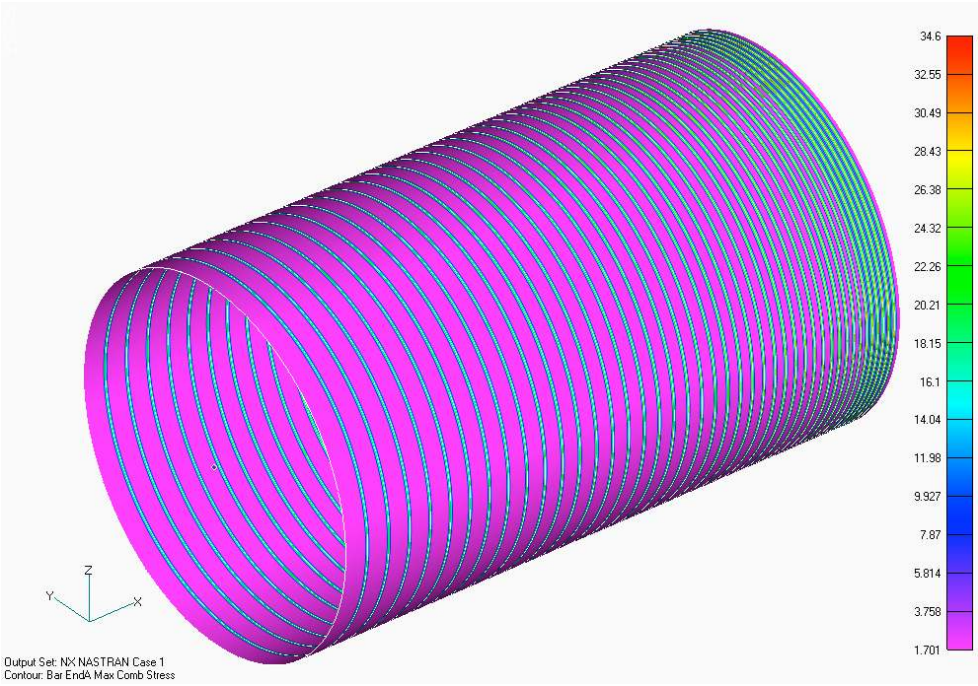


Figure 16 Frames maximum stress for the pressurization case [×10MPa].

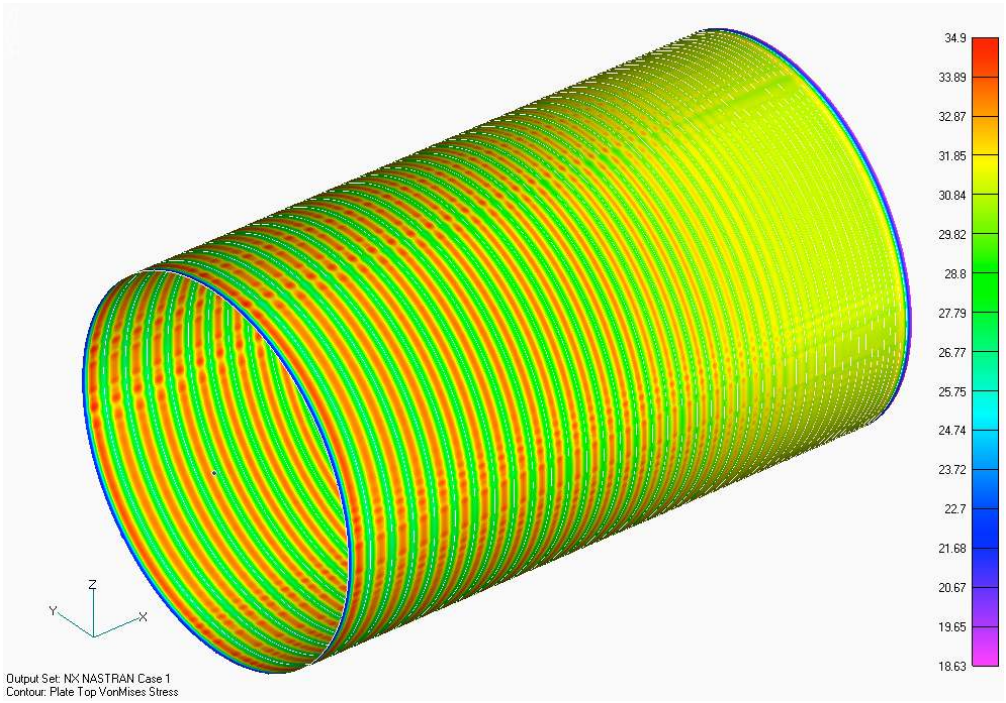


Figure 17 Panel Von Mises stress for the pressurization case [×10MPa].

The maximum stress equals to 346 MPa in the frames and 349 MPa in the reinforced panels, which is below the material ultimate tensile stress ($F_{tu} = 469$ MPa), indicating that the fuselage structure withstands its ultimate pressurization load. This first numerical analysis demonstrates that, despite the fuselage has been designed based on a reinforced panels under compressive loads criterion, the resulting structure supports its most severe tensile requirement also.

Figure 18 presents the stresses acting in the longitudinal x-direction of the aircraft, for the pull-up maneuver load case, according to the loading distributions of Figs. 8 and 9, resulting in compression at the bottom reinforced panels and tension at the top of the fuselage, as predicted.

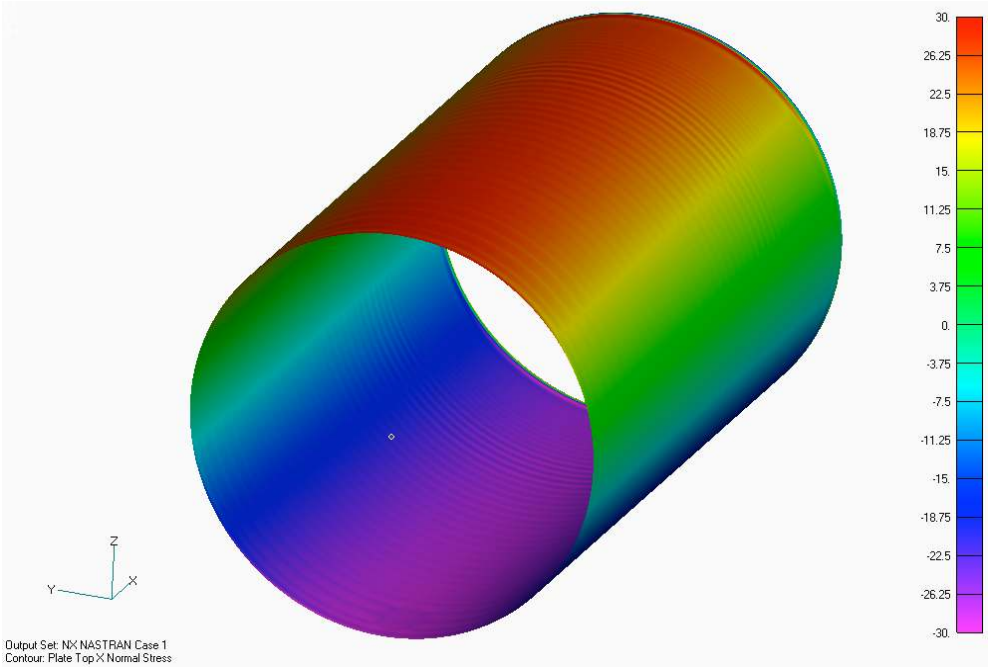


Figure 18 Stress in the longitudinal x-direction – Global Model [×10MPa].

The compressive stresses of the lower reinforced panels are almost constant along the whole span of the central fuselage, varying from 270 MPa up to 300 MPa. This interval is in accordance with the compressive allowable stresses to the reinforced panels metamodel, Tab 1. Therefore, this finite element analysis demonstrates that the analytical procedure is consistent and valid. The compressive stresses throughout the lower fuselage are around 2/3 of the compressive yield stress, which implies that the structure is globally optimized, avoiding local instability failures at stresses far below the material yield compressive limit.

A detailed local model is prepared to enable the accurate buckling analysis, since the instability failure plays a main hole in this sizing procedure. Displacements and loads extracted from the global FE model provide the input data for the refined local model. Figure 19 shows the stresses acting in the longitudinal x-direction of the aircraft.

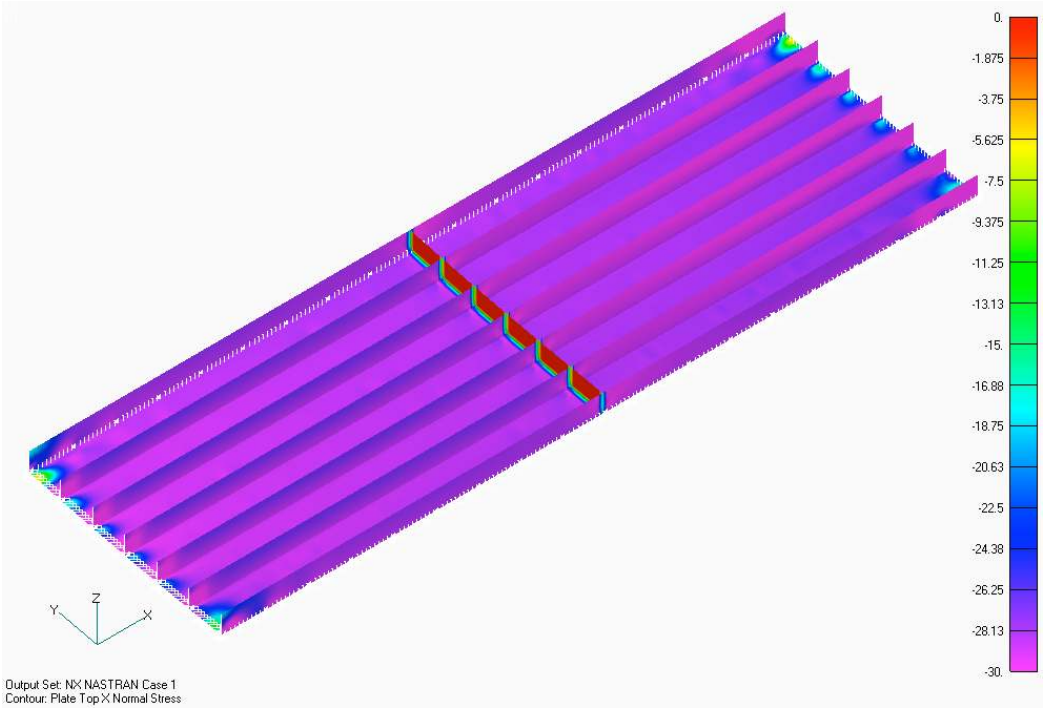


Figure 19 Stress in the longitudinal x-direction – Local Model [×10MPa].

Despite the presence of certain singularities observed in the intersections of frames with stringers at the ends of the detailed local model due to the boundary conditions and applied loads, the compressive stress level remains similar to that obtained in the global model, between 270 MPa and 300 MPa.

The six first buckling modes and their respective eigenvalues λ, representing the ratio of the buckling load by the acting load, are presented in Fig. 20. The first two buckling modes occurred in a region where high concentrated stresses can be observed in Fig. 19, due to non-physical behavior caused by the transfer of the global displacements and loads to the detailed local model. Thus, they represent spurious modes and are disregarded. The buckling loads to the first modes are very close, indicating that the collapse of the structure occurs when its critical load is reached without an extra margin for post-buckling effects.

Another important point is the occurrence of simultaneous failure in stringers and skin in large portions of the panel, indicating the simultaneous collapse of the structure. But it was not possible to visualize the panel buckling as a column in these first failure modes. If the stiffness provided by actual fuselage frames is significantly higher than that of a simply supported column, then the compressive allowable stress will be a little higher than that calculated by the metamodeling hypotheses.

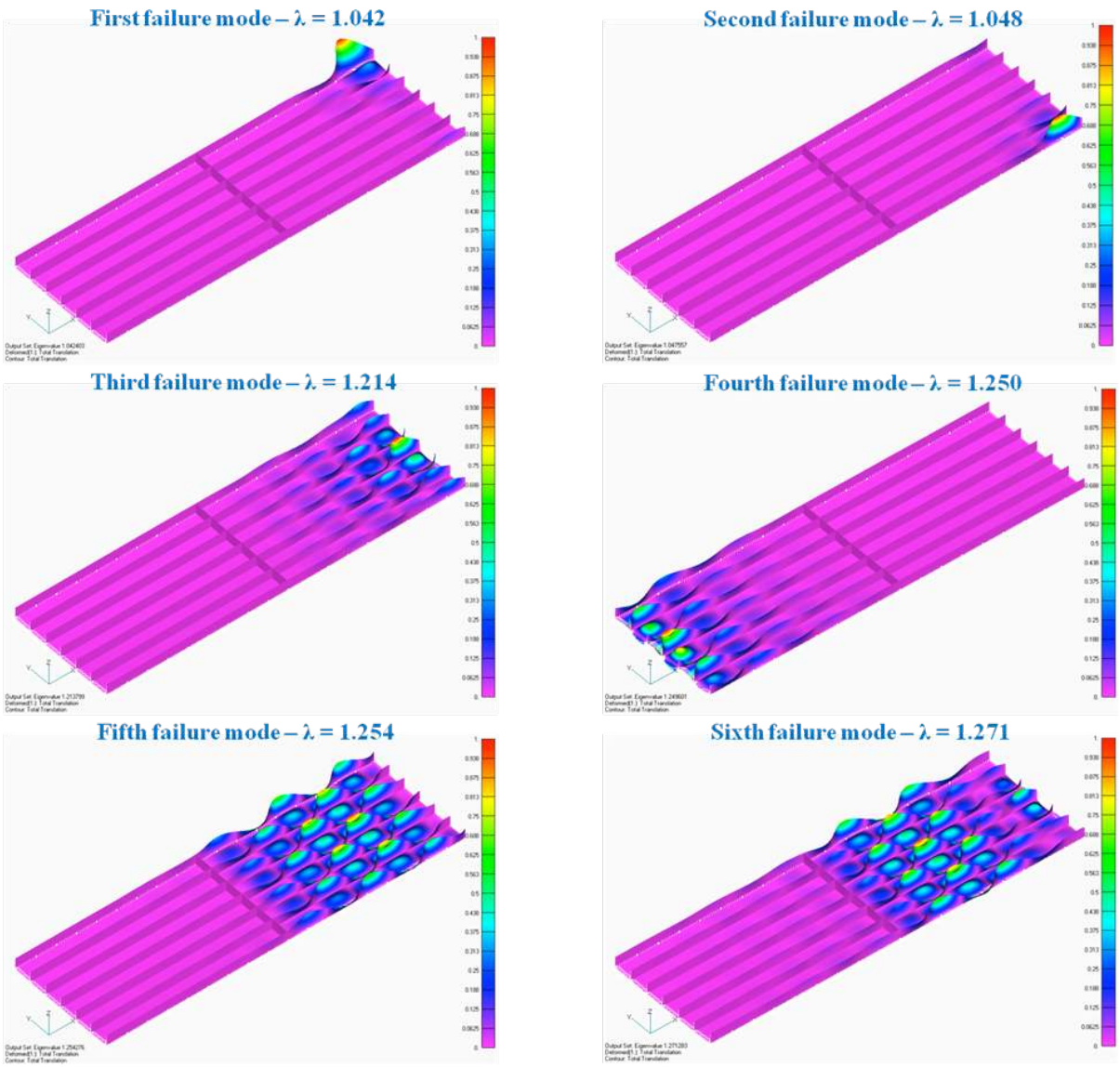


Figure 20 Failure modes – Local Model.

It is also evident that the compressive strength of the structure is at least 21.4% higher than the fuselage acting loads, resulting in margins of safety greater than those obtained by the analytical method. This difference may be explained by some conservative hypotheses adopted during the pre-sizing of the fuselage:

- the presented methodology is conservative when it assumes that the skin is sized as a simply supported plate and the stringers as simply supported flanges;
- the analytical methodology is developed for flat panels, while the fuselage possesses curved panels. However, the dimensions of the panels are small compared to the curvature radius of the fuselage and, in this case, the buckling coefficient for curved panels is approximately equal to that of flat panels;

- buckling FE simulation to the flat reinforced panels demonstrated a compressive strength 3.6% greater than analytical predicted, Fig. 4.

Throughout this specific application, some simplifications and hypotheses have been adopted. Thus, opportunities are identified for future investigation to this new fuselage concept:

- a dedicated procedure for dimensioning the fuselage ceiling reinforced panels, subjected to tensile stresses, mainly governed by fatigue and damage tolerance criteria;
- a study of local reinforcements for fuselage openings, in order to accommodate windows and doors.

4 CONCLUSION

An efficient metamodel for reinforced panels under compressive loads, typically used in light-weight aircraft structures, has been proposed. The metamodel represents a replicable cell of wing box or fuselage composed of integrally machined panels. The presented analytical formulation for the conception of reinforced panels under compressive loads is based on the synthesis of four stability criteria: section crippling, web buckling, flange buckling and column collapse. The aluminum alloy AL7050-7451 Plate 2.75in, a typical choice in modern aircraft industry, is selected to the reinforced panel metamodel. The structure is expected to work in the linear elastic domain.

The local buckling of the skins is usually allowed and the sizing of the stringers and frames is performed taking into account the post buckling behavior of the panels. In the methodology adopted herein, the buckling modes occur simultaneously, causing the collapse of the whole structure, so the structure can not buckle at all.

The numerical applications show that the geometry of the basic structural components of a fuselage can be easily and quickly determined by means of the presented methodology. The consistency and validity of the methodology is demonstrated by finite element analyses.

The design of a 9-passenger aircraft fuselage yields to an innovative structure from those usually adopted in the aeronautical industry. The resulting geometry alludes to a reticulated pattern of the structure. It is an option and a trend that can lead to new aerospace structures. Although, the small dimensions and spacing of the structural elements found herein make the fuselage manufacturing unfeasible considering current processes in the aeronautical industry nowadays. It is expected that the presented formulation could be more helpful to the pre-sizing of structures subjected to higher compressive loads, such as in the case of the upper skin panels of a wing box.

References

Abaqus (2006). User's Manual.

Alinia, M.M., Habashi, H.R., Khorram, A. (2009). Nonlinearity in the postbuckling behaviour of thin steel shear panels. Thin-Walled Structures 47, 412–420.

Bedair, O.K. (1997). The Elastic Behaviour of multi-stiffened plates under uniform compression. Thin-Walled Structures, 27-4, 311-335.

Bruhn, E.F. (1973). Analysis and design of flight vehicle structures. Purdue: Jacobs Pub.

Campbell, J., Hetey, L., Vignjevic, R. (2012). Non-linear idealization error analysis of a metallic stiffened panel loaded in compression. Thin-Walled Structures 54, 44-53.

Caseiro, J.F., Valente, R.A.F., Andrade-Campos, A., Yoon, J.W. (2011). Elasto-plastic buckling of integrally stiffened panels (ISP): An optimization approach for the design of cross-section profile. Thin-Walled Structures, 49, 864–873.

Federal Aviation Regulations – Part 25 (2011). Airworthiness Standards – Transport Category Airplanes – Subpart C – Structures. Federal Aviation Administration.

Forrester, A.I.J. , Sóbester, A. , Keane, A.J. (2008). Engineering design via Surrogate Modelling: A practical Guide. Progress in Astronautics and Aeronautics, vol. 226, John Wiley and Sons.

Gerard, G. (1958). The Crippling Strength of Compression Elements. Jour. Aeronaut. Science, v 25 (1), 37-52.

http://www.engineering.leeds.ac.uk/documents/InauguralLecture_VT_short.ppt.

Kolakowski, Z. and Teter, A. (2000). Interactive buckling of thin-walled beam-columns with intermediate stiffeners or/and variable thickness. International Journal of Solids and Structures 37, 3323-3344.

Lee, J. and Kang, S. (2007). GA based meta-modeling of BPN architecture for constrained approximate optimization. International Journal of Solids and Structures 44, 5980-5993.

Lundquist, E. and Stowell, E. (1941). Critical Compressive Stress for Outstanding Flanges. Report No. 734. Langley Memorial Aeronautical Laboratory, National Advisory Committee for Aeronautics. Langley Field, VA.

Lynch, C., Murphy, A., Price, M., Gibson, A. (2004). The computational post buckling analysis of fuselage stiffened panels loaded in compression, Thin-Walled Structures, 42 , 1445-1464.

MSC.Nastran, (2004). MSC.Software, Reference Manual.

Smith, J., Hodgins, J., Oppenheim, I., Witkin, A. (2013). Creating Models of Truss Structures with Optimization, Carnegie Mellon University and Pixar Animation Studios, http://www.smokingrobot.com/pdfs/SIG02_structures.pdf.

Stamatelos, D.G., Labeas, G.N., Tserpe, K.I. (2011). Analytical calculation of local buckling and post-buckling behavior of isotropic and orthotropic stiffened panels. Thin-Walled Structures 49, 422–430.

Timoshenko, S. and Gere, J. (1961). Theory of Elastic Stability. McGraw-Hill.

Toropov, V. (2013). Optimization: getting more and better for less, inaugural lecture, aerospace and structural engineering, University of Leeds,

Wang, Q. (1997). Lateral buckling of thin-walled open members with shear lag using optimization techniques. International Journal of Solids and Structures, 34-11, 1343-1352.

Yoon, J.W., Bray, G.H., Valente, R.A.F., Childs, T.E.R. (2009). Buckling analysis for an integrally stiffened panel structure with a friction stir welding. Thin-Walled Structures 47, 1608–1622.